Copyright © 1998, American Institute of Aeronautics and Astronautics, Inc.

A98-39895

AIAA-98-4950

TOPOLOGY OPTIMIZATION OF GEOMETRICALLY NONLINEAR STRUCTURES AND COMPLIANT MECHANISMS

Tyler E. Bruns and Daniel A. Tortorelli *
Department of Mechanical and Industrial Engineering
University of Illinois at Urbana-Champaign
Urbana, Illinois 61801

Abstract

Topology optimization of structures has become an area of rapidly increasing interest to researchers during the past decade. Most structural topology optimization problems assume a linear elastic response. This assumption is not valid for systems undergoing large deformation. The structural analysis here accommodates geometric and material nonlinearities, and its impact on the topology optimization is investigated. A well-posed regularized topology optimization problem is developed by introducing a Gaussian-weighted density measure. Topology results based on the linear and nonlinear elastic formulations are compared. The formulation of the structural design problem is then extended to design compliant mechanisms undergoing large displacements.

1. Introduction

With the proliferation of high speed computing, the automated analysis of structures and mechanisms has become routine. However, designers continue to rely on traditional trial and error and ingenuity to synthesize structures and mechanisms. Consequently, researchers have turned their attention to the more difficult task of automating the tedious aspects of the creative design process. Designers that follow classical design procedures employ heuristic approaches to generate novel concepts and incrementally improve tested ideas. In contrast, a modern approach incorporates computer-aided analysis tools with analytical design sensitivity analysis and numerical optimization.

The goal of the structural topology problem[1,2] is to determine an optimal distribution of material within a design domain while satisfying a desired objective. The prescribed domain is typically defined by a ground structure discretized by finite elements. Here, we investigate the distribution of material ranging from solid to void at every point within a continuum ground structure. An alternative approach is to vary the cross-sectional properties of truss elements in a ground structure.

Analysis techniques for rigid multibody dynamics have matured, and systematic formulations to analyze flexible multibody systems have attracted large interest from the structural dynamics and the multibody dynamics communities.[3,4] The synthesis of mechanisms through design sensitivity and numerical optimization techniques has become an area of considerable research.[5,6] These problems are cast as sizing optimization problems, although some investigation into shape optimization has been done. In addition, some research has addressed the issue of rigid body mechanism topology based on graph theory.[7] However, systematic formulations to automate the difficult task of synthesizing the topology of flexible multibody systems have not been formulated.

A promising approach to synthesize the topology of flexible mechanisms has been developed from structural topology optimization.[8,9] Unlike structural optimization where mechanism-like modes of deformation are undesirable, these modes are sought in the topology optimization of compliant mechanisms. Compliant mechanisms admit a limited range of motion primarily due to elastic deformation in contrast to multibody mechanisms which allow large relative motion due to their joint. Both the truss and continuum ground structure approaches have been used to generate compliant mechanisms. Here, however, only the continuum approach is discussed. *

*Also, Department of Theoretical and Applied Mechanics

*The pseudo-rigid-body model[10] is also used to design

Copyright © 1998, American Institute of Aeronautics and Astronautics, Inc.

Most formulations for structural topology optimization are based on linear elastic assumptions, i.e. small displacement gradients. This assumption is applicable to a large variety of problems. However, even if the system experiences small relative deformation while undergoing large overall motion, as is the case in space antennas or mechanisms, then the linear elastic assumption is invalid. The present topology investigation accommodates geometric and material nonlinearities. It is used to design structures and compliant mechanisms.

In Section 2 an overview of the solid mechanics problem is presented. The structural topology optimization problem is given in Section 3. Topology syntheses of geometrically nonlinear structures and compliant mechanisms are presented in Sections 4 and 5.

2. Nonlinear Hyperelastic Analysis

An overview of the solid mechanics boundary value problem is developed. The boundary value problem is initially posed in its strong form and recast to an equivalent weak form for finite element discretization. The resulting set of simultaneous nonlinear equations are solved iteratively using the Newton Raphson method.

2.1 Boundary Value Problem

A particle located by the position vector $\mathbf{X}$ in the undeformed body configuration $\mathrm{V_o}$ experiences the displacement $\mathbf{u}$. The symmetric Green-St. Venant strain tensor $\mathbf{E}$ is defined through the deformation gradient $\mathbf{F}$.

$$\mathbf{F}(\mathbf{X}) = \mathbf{I} + \nabla\mathbf{u}(\mathbf{X}) \quad (1)$$

$$\mathbf{E}(\mathbf{X}) = \frac{1}{2}(\nabla\mathbf{u}(\mathbf{X}) + \nabla^{\mathrm{T}}\mathbf{u}(\mathbf{X}) + \nabla^{\mathrm{T}}\mathbf{u}(\mathbf{X})\nabla\mathbf{u}(\mathbf{X})) \quad (2)$$

If the strain is linearized, then the higher order geometric stiffening term is neglected.

We assume that the inertial effects are negligible, i.e. the system response is treated as quasi-steady-state and hence the equations of local linear and angular balance give

$$\mathrm{div}\,(\mathbf{F}(\mathbf{X})\mathbf{T_o}(\mathbf{X})) + \mathbf{b_o}(\mathbf{X}) = \mathbf{0} \quad (3)$$

$$\mathbf{T_o}(\mathbf{X}) = \mathbf{T_o^T}(\mathbf{X}) \quad (4)$$

where the symmetric 2^{nd} Piola-Kirchhoff stress tensor is denoted by $\mathbf{T_o}$, and the body forces are expressed as $\mathbf{b_o}$.

It is assumed that the material behaves hyperelastically, i.e. the material response is path independent and can be derived from a strain energy function e defined on the undeformed configuration; its derivative $\mathbf{C}$ is the elasticity tensor. If we assume that the structure and later the compliant mechanism experience small strains despite undergoing large displacement, a St. Venant-Kirchhoff material behavior is applicable. Here, we augment this material with a nonlinear function of the determinant of the Green-St. Venant strain tensor h to enforce stability of the solid material undergoing large displacement.

$$\mathbf{T_o}(\mathbf{X}) = \frac{\partial e}{\partial \mathbf{E}}(\mathbf{E}(\mathbf{X})) = \mathbf{C}(\mathbf{E}(\mathbf{X}))\mathbf{E}(\mathbf{X}) \quad (5)$$

$$e(\mathbf{E}(\mathbf{X})) = \frac{\nu \mathrm{E}}{2(1+\nu)(1-2\nu)}\mathrm{tr}(\mathbf{E}(\mathbf{X}))^2 + \frac{\mathrm{E}}{2(1+\nu)}\mathrm{tr}(\mathbf{E}(\mathbf{X})^2) + \beta h(\det(\mathbf{E}(\mathbf{X}))) \quad (6)$$

The strain energy function e for an isotropic St. Venant-Kirchhoff material depends on two material parameters, i.e. Young's modulus E and Poisson's ratio ν. When β is nonzero, the nonlinear function h is active, otherwise a linear elastic material behavior (with nonlinear strain) is used.

Displacement and surface traction boundary conditions are prescribed as $\mathbf{u}^{\mathrm{p}}$ and $\mathbf{t}^{\mathrm{p}}$ on the complementary boundaries $\mathrm{A_o^u}$ and $\mathrm{A_o^t}$ of the body. The prescribed surface tractions $\mathbf{t}^{\mathrm{p}}$ are prescribed on the undeformed configuration.

$$\mathbf{u}(\mathbf{X}) = \mathbf{u}^{\mathrm{p}}(\mathbf{X}) \qquad \mathbf{X} \in \mathrm{A_o^u} \quad (7)$$

$$\mathbf{F}(\mathbf{X})\mathbf{T_o}(\mathbf{X})\mathbf{n_o}(\mathbf{X}) = \mathbf{t}^{\mathrm{p}}(\mathbf{X}) \qquad \mathbf{X} \in \mathrm{A_o^t} \quad (8)$$

The objective of the boundary value problem is to determine the displacement field $\mathbf{u}$.

2.2 Variational Formulation

The boundary value problem is recast in an equivalent variational form. The scalar residual g is formed by multiplying equations 3 and 8 by a weighting function $\mathbf{v}$ and integrating over the regions $\mathrm{V_o}$ and $\mathrm{A_o^t}$. The prescribed displacement boundary conditions are accommodated by restricting $\mathbf{u}$ and $\mathbf{v}$ to the set of kinematically admissible displacements. The symmetry of equation 4 is enforced by our selection of material constitutive law. After application

compliant mechanisms.

Copyright © 1998, American Institute of Aeronautics and Astronautics, Inc.

of integration by parts and the divergence theorem, the residual is expressed in a equivalent weak form.

$$\begin{aligned} g(\mathbf{u}) &= 0 \qquad (9) \\ &= -\int_{V_o} \nabla \mathbf{v} \cdot (\mathbf{F}\mathbf{T_o})\, dV_o + \\ &\quad \int_{V_o} \mathbf{v} \cdot \mathbf{b_o}\, dV_o + \int_{A_o^t} \mathbf{v} \cdot \mathbf{t}^{\mathbf{p}}\, dA_o \qquad (10) \end{aligned}$$

This form is readily suited for finite element discretization.

2.3 Newton Raphson Method

Although other iterative methods are available, the Newton Raphson method is implemented due to its quadratic convergence and due to its use in the design sensitivity analysis.

The set of discretized nonlinear governing equations $\mathbf{G}$ dependent on the discretized response field $\mathbf{U}$ are expressed in residual form.

$$\mathbf{G}(\mathbf{U}) = \mathbf{0} \qquad (11)$$

A Taylor series expansion is performed about the current response $\mathbf{U}_i$ to update the response $\mathbf{U}_{i+1} = \mathbf{U}_i + \triangle\mathbf{U}$ so that to first-order $\mathbf{G}(\mathbf{U}_{i+1}) = \mathbf{0}$.

$$\mathbf{K}_T(\mathbf{U}_i)\triangle\mathbf{U} = \mathbf{G}(\mathbf{U}_i) \qquad (12)$$

$$\mathbf{K}_T(\mathbf{U}_i) \equiv -\frac{\mathbf{DG}}{\mathbf{DU}}(\mathbf{U}_i) \qquad (13)$$

where $\mathbf{K}_T$ is the tangent matrix. The update strategy is continued until convergence is met.

2.4 Finite Element Discretization

The displacement field $\mathbf{u}$ is discretized by finite elements using spatial dependent shape functions $\mathbf{N}$ and response dependent nodal displacements $\mathbf{U}$.

$$\mathbf{u} = \mathbf{N}\,\mathbf{U} \qquad (14)$$

Upon substitution of equation 14 into 10, the discrete form of the residual $\mathbf{G}$ is expressed as

$$\mathbf{G}(\mathbf{U}) = \mathbf{0} = \mathbf{S}(\mathbf{U}) + \mathbf{F} \qquad (15)$$

where $\mathbf{S}$ represents internal forces and $\mathbf{F}$ represents external forces. The displacements are further partitioned into unknown free displacements $\mathbf{U}^f$ and known prescribed displacements $\mathbf{U}^p$.

$$\mathbf{U} = \left\{ \begin{array}{c} \mathbf{U}^f \\ \mathbf{U}^p \end{array} \right\} \qquad (16)$$

Consequently, the governing equations are partitioned into the $\mathbf{G}^{\mathbf{f}}$ and $\mathbf{G}^{\mathbf{p}}$ residual vectors as

$$\begin{aligned} \mathbf{G}(\mathbf{U}^p, \mathbf{U}^f) &= \left\{ \begin{array}{c} \mathbf{G}^{\mathbf{f}}(\mathbf{U}^p, \mathbf{U}^f) \\ \mathbf{G}^{\mathbf{p}}(\mathbf{U}^p, \mathbf{U}^f) \end{array} \right\} \\ &= \left\{ \begin{array}{c} \mathbf{S}^f(\mathbf{U}^p, \mathbf{U}^f) \\ \mathbf{S}^p(\mathbf{U}^p, \mathbf{U}^f) \end{array} \right\} + \left\{ \begin{array}{c} \mathbf{P} \\ \mathbf{R} \end{array} \right\} \\ &= \mathbf{0} \qquad (17) \end{aligned}$$

where $\mathbf{P}$ and $\mathbf{R}$ are the applied and reaction forces, respectively.

The first set of simultaneous nonlinear equations $\mathbf{G}^{\mathbf{f}}$ are solved for the unknown free displacements $\mathbf{U}^f$ using the Newton Raphson method. As previously noted, dead loading is assumed so that $\mathbf{P}$ is independent of the response. However, live loading can be easily accommodated in this nonlinear formulation. The tangent stiffness matrix $\mathbf{K}_T$ results from differentiating the nonlinear residual $\mathbf{G}^{\mathbf{f}}$ with respect to the free displacements $\mathbf{U}^f$.

$$\mathbf{K}_T = -\frac{\partial \mathbf{G}^{\mathbf{f}}}{\partial \mathbf{U}^f}(\mathbf{U}^p, \mathbf{U}^f) \qquad (18)$$

Once the free displacements are solved, the unknown reaction forces $\mathbf{R} = -\mathbf{S}^{\mathbf{p}}$ are computed through the algebraic residual $\mathbf{G}^{\mathbf{p}}$.

3. Topology Optimization

The goal of the structural topology problem is to determine an optimal distribution of material within the design domain that satisfies some desired objective. Here, the prescribed domain is defined by a continuum ground structure discretized by finite elements. The topology design problem, i.e. to obtain a solid material and void distribution, is most naturally posed as an integer programming problem. However, the discrete-valued design problem is recast as one with continuously varying density design variables to take advantage of computationally efficient nonlinear programming methods. Two approaches to formulate a well-posed, regularized problem have been forwarded: 1. methods that expand the design space by introducing composite material, i.e. the homogenization method,[11] and 2. methods that restrict composite material from the design space, e.g. approaches with perimeter control[12] or slope constraints.[13] We seek topologies that are comprised of solid material and void rather than perforated microstructure, so we follow the latter approach.

The topology optimization is prone to numerical instabilities[14] as evident by the checkerboard

Copyright © 1998, American Institute of Aeronautics and Astronautics, Inc.

patterns that appear when penalizing intermediate densities. In addition, different topologies may result due to mesh refinement. Furthermore, a large number of local minima in the design space prevent the numerical optimization algorithms from reaching better solutions and result in different topologies based on different initial density distributions. These issues are addressed by formulating a well-posed, regularized problem.

3.1 Density Measure

A density design variable d_i (component i of the design variable vector $\mathbf{d}$) ranging from solid material, i.e. $d_i = 1$, to void, i.e. $d_i = 0$, is assigned to each finite element i by the optimization algorithm. The material distribution, i.e. topology of the domain, evolves as the optimization algorithm attempts to satisfy the desired objective.

Here, the material density is introduced into the topology optimization by weighting the elasticity tensor $\mathbf{C}$ in each element i by a density measure, $\bar{\eta}(\mathbf{d})$, i.e.

$$\bar{\mathbf{C}}(\mathbf{E}, \mathbf{d}) = \{\gamma + (1-\gamma)\bar{\eta}^{\mathrm{P}}(\mathbf{d})\}\mathbf{C}(\mathbf{E}) \qquad (19)$$

A lower bound on the elasticity tensor, $\gamma\mathbf{C}$, ensures that the tangent matrix $\mathbf{K}_T$ does not become singular due to void material. A penalty parameter $p \geq 1$, which is incremented throughout the optimization via a continuation method, penalizes less efficient intermediate densities.

In some formulations, the density measure $\bar{\eta}(\mathbf{d})$ in each element i is simply defined by the element density design variables, i.e. $\bar{\eta}(\mathbf{d}) = d_i$. Unfortunately, checkerboard patterns appear when the density measure is penalized by a parameter p greater than 1 (see Figure 1). To prevent the checkerboard pattern, a global perimeter constraint or local slope constraints are imposed to regularize the problem. The regularization has the effect of constraining the connectivity of the topology.

Figure 1: Checkerboard pattern.

Here, the density measure for element i is defined by a Gaussian kernal over the surrounding region. Therefore, the density design variables $\mathbf{d}$ are determined via the optimization, but the regularization is accommodated through $\bar{\eta}$ and equation 19. For each element i, the Gaussian distribution is based on the distance of the surrounding element j centroids (x_j, y_j) within a fixed mesh-independent radius r of the element i centroid (x_i, y_i).

$$\bar{\eta}(\mathbf{d}) = \sum_j \frac{\omega_j}{\omega} d_j \qquad (20)$$

$$\omega_j = \frac{1}{2\pi r^2} \mathrm{e}^{\frac{-(x_j-x_i)^2+(y_j-y_i)^2}{2r^2}} \qquad (21)$$

$$\omega = \sum_j \omega_j \qquad (22)$$

The advantage of this approach is that the regularization is accommodated directly without imposing additional slope or perimeter constraints in the optimization problem. The drawback of the approach is that equilibrium is satisfied by the density measures rather than the density design variables; consequently the optimization result is not readily interpreted, rather it must obtained from the function $\bar{\eta}$. Fortunately, the topologies given directly by $\mathbf{d}$ and by $\bar{\eta}(\mathbf{d})$ are comparable as depicted in Figures 2 and 3.

Figure 2: Topology plot of the density measures, $\bar{\eta}(\mathbf{d})$.

Figure 3: Topology plot of the density design variables, $\mathbf{d}$.

3.2 Numerical Optimization

The large number of design variables in the topology optimization problem necessitates the use of large-scale optimization algorithms. The Method of Moving Asymptotes (MMA)[15] is a computationally efficient nonlinear programming method based on gradient information. † A suitable objective function Θ_1 subject to inequality or equality constraints

†The restriction to the feasible region hinders the solution of the topology optimization problem, particularly in the case of mass constraints. Artificial variables are introduced in the

Copyright © 1998, American Institute of Aeronautics and Astronautics, Inc.

Θ_i (for $i = 2, \ldots$) is minimized in the topology optimization problem. The objective function and constraint responses Θ_i are functions of the bounded design variables d_j, (for $j = 1, 2, \ldots$). The topology optimization problem is posed in the following form.

$$\begin{aligned} \text{minimize} \quad & \Theta_1(\mathbf{d}) && (23)\\ \text{subject to} \quad & \Theta_i(\mathbf{d}) \leq \mathbf{0} && (24)\\ & {d_j}^{LB} \leq d_j \leq {d_j}^{UB} && (25) \end{aligned}$$

3.3 Design Sensitivity Analysis

The combination of a large number of design variables and a computationally intensive nonlinear analyses requires the efficient calculation of analytical sensitivities.[16,17] Analytical sensitivities are calculated here by the adjoint method. This method is well suited for problems with a large number of design variables compared to the number of response functions. The efficiency of the method is due to elimination of the state sensitivity calculations, i.e. $\frac{\mathrm{D}\mathbf{U}^f}{\mathrm{D}d_j}$ and $\frac{\mathrm{D}\mathbf{R}}{\mathrm{D}d_j}$, by posing an adjoint problem and due to the use of the previously decomposed tangent stiffness matrix from the primal analysis.

The adjoint formulation for structural optimization begins by premultiplying the respective governing equations, i.e. equation 17, by Lagrange multipliers $\boldsymbol{\lambda}^f$ and $\boldsymbol{\lambda}^p$ and appending these terms to the response functions Θ_i. Note that the values of the augmented response functions $\hat{\Theta}_i$ equal that of the original response functions Θ_i as the residual terms equal zero.

$$\begin{aligned} \hat{\Theta}_i(\mathbf{d}) = \; & \Theta_i(\mathbf{U}^p(\mathbf{d}), \mathbf{U}^f(\mathbf{d}), \mathbf{R}(\mathbf{d}), \mathbf{d}) + \\ & {\boldsymbol{\lambda}^f}^{\mathrm{T}} \mathbf{G}^{\mathrm{f}}(\mathbf{U}^p(\mathbf{d}), \mathbf{U}^f(\mathbf{d}), \mathbf{d}) + \\ & {\boldsymbol{\lambda}^p}^{\mathrm{T}} (\mathbf{S}^p(\mathbf{U}^p(\mathbf{d}), \mathbf{U}^f(\mathbf{d}), \mathbf{d}) + \mathbf{R}(\mathbf{d})) \end{aligned} \quad (26)$$

The analytical sensitivities are obtained by differentiating the response functions $\hat{\Theta}_i$ with respect to each design variable d_j. By collecting and eliminating the coefficients of the state sensitivities, i.e. $\frac{\mathrm{D}\mathbf{U}^f}{\mathrm{D}d_j}$ and $\frac{\mathrm{D}\mathbf{R}}{\mathrm{D}d_j}$, the adjoint problem is formed. The Lagrange multipliers $\boldsymbol{\lambda}^f$ and $\boldsymbol{\lambda}^p$ are evaluated by solving the adjoint problem once for each response function Θ_i. Note that the tangent stiffness matrix has been previously assembled and decomposed during the primal analysis, so an efficient back substitution is all that is required to determine $\boldsymbol{\lambda}^f$.

$$\begin{aligned} \boldsymbol{\lambda}^p &= -\frac{\partial \Theta_i}{\partial \mathbf{R}}^{\mathrm{T}} (\mathbf{U}^p(\mathbf{d}), \mathbf{U}^f(\mathbf{d}), \mathbf{R}(\mathbf{d}), \mathbf{d}) \\ {\mathbf{K}_T}^{\mathrm{T}}(\mathbf{d}) \boldsymbol{\lambda}^f(\mathbf{d}) &= \frac{\partial \Theta_i}{\partial \mathbf{U}^f}^{\mathrm{T}} (\mathbf{U}^p(\mathbf{d}), \mathbf{U}^f(\mathbf{d}), \mathbf{R}(\mathbf{d}), \mathbf{d}) \\ &\quad + \frac{\partial \mathbf{S}^p}{\partial \mathbf{U}^f}^{\mathrm{T}} (\mathbf{U}^p(\mathbf{d}), \mathbf{U}^f(\mathbf{d}), \mathbf{d}) \boldsymbol{\lambda}^{\mathrm{P}}(\mathbf{d}) \end{aligned} \quad (27)$$

The response sensitivities $\frac{\mathrm{D}\hat{\Theta}_i}{\mathrm{D}d_j}$ are then calculated as follows.

$$\begin{aligned} \frac{\mathrm{D}\hat{\Theta}_i}{\mathrm{D}d_j} = \; & \frac{\partial \Theta_i}{\partial \mathbf{U}^p} \frac{\mathrm{D}\mathbf{U}^p}{\mathrm{D}d_j} + \frac{\partial \Theta_i}{\partial d_j} + \\ & {\boldsymbol{\lambda}^f}^{\mathrm{T}} \left(\frac{\partial \mathbf{G}^{\mathrm{f}}}{\partial \mathbf{U}^p} \frac{\mathrm{D}\mathbf{U}^p}{\mathrm{D}d_j} + \frac{\partial \mathbf{G}^{\mathrm{f}}}{\partial d_j} \right) + \\ & {\boldsymbol{\lambda}^p}^{\mathrm{T}} \left(\frac{\partial \mathbf{S}^p}{\partial \mathbf{U}^p} \frac{\mathrm{D}\mathbf{U}^p}{\mathrm{D}d_j} + \frac{\partial \mathbf{S}^p}{\partial d_j} \right) \end{aligned} \quad (28)$$

4. Geometrically Nonlinear Structures

The topology optimization problem is posed to design structures undergoing large displacement, and a comparison between the topologies due to the nonlinear and linear elasticity formulations is presented. The results address the limitations of the linear assumption and motivate the necessity of a nonlinear formulation to accommodate large displacements.

The usual objective in the design of a structure is to minimize the compliance, or maximize the stiffness, under prescribed loading conditions. In addition, an upper bound constraint is placed on the mass m of the structure to limit resources. The density design variables are allowed to vary between solid material and void. With regard to equations 23–25,

$$\begin{aligned} \Theta_1 &= \mathbf{P}^{\mathrm{T}}\mathbf{U}^f + \mathbf{R}^{\mathrm{T}}\mathbf{U}^p && (29)\\ \Theta_2 &= m - m^{UB} && (30)\\ {d_j}^{LB} &= 0 && (31)\\ {d_j}^{UB} &= 1 && (32) \end{aligned}$$

The topology design of a cantilever beam (refer to Figure 4) is investigated. A dead load P is applied to the beam tip. The $200mm \times 100mm$ domain is discretized by 1600 4-noded quadrilateral elements. The material response is given by equation 6 where the Young's modulus $E = 3000N/mm^2$, the Poisson's ratio $\nu = 0.4$, and the material behavior parameter $\beta = 0$.

MMA optimization algorithm to prevent its subproblem from becoming infeasible.[15] However, active constraints that are highly dependent on parameters that are varied via continuation methods, e.g. the penalty parameter p, can cause the design to become infeasible.

Copyright © 1998, American Institute of Aeronautics and Astronautics, Inc.

The initial density design variables are set to $d_j = 0.3$. The penalty parameter p is incremented in steps of 0.1 from 1.5 to 3.0. The upper bound on the resource constraint, m^{UB} is set to 40% of the original domain mass, hence the initial design is feasible.

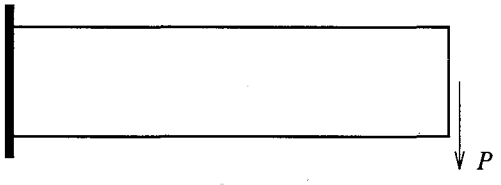

Figure 4: Tip-loaded cantilever beam.

A symmetric topology due to the linear analysis at $P = 1N$ is obtained. The density measures $\bar{\eta}(\mathbf{d})$ for this design are depicted in Figure 5. The response and response gradients are linearly scaled by P for loads $P > 1$, and therefore, the same symmetric topology is expected for each load level.

The density measures for the optimal topologies due to the nonlinear analysis are plotted in their deformed configurations in Figures 6–11. Note that similar topologies occur for the linear and nonlinear topology optimizations at $P = 1N$, cf. Figures 5 and 6. However, as the load is increased, the topology becomes progressively unsymmetric cf. Figures 7–9. At larger loads and corresponding larger displacements, entirely new topologies result, cf. Figures 10 and 11.

Figure 5: Topology plot of the density measures, $\bar{\eta}(\mathbf{d})$. Linear elastic analysis with $P = 1N$.

The compliance of the topology design shown in Figure 5 is $2.038 \times 10^{-2} Nmm$. The topology design is due a linear elastic analysis with a load of $P = 1N$. The compliance results due to loads $P > 1N$ are easily calculated by scaling the results due to the load $P = 1N$. However, the linear assumption is violated for loads $P \gg 1N$.

In Table 1, a comparison of compliance results for the topology designs is presented. The second column lists the compliance for nonlinear elastic analyses of the topology design shown in Figure 5. Nonlinear elastic analyses are performed for 6 load cases between $P = 1N$ and $1000N$. Recall that the topology is generated by a linear elastic analysis. The third column lists the compliance results due to the topologies shown in Figures 6–11. For these 6 cases, nonlinear elastic analyses are performed. As seen in Table 1, if the design is based on linear elastic analysis, but nonlinear deformations are present, then it is possible to improve the compliance of the structure. Albeit, the differences are not extreme for this example.

	Compliance (Nmm)	
P (N)	Nonlinear Elastic Analysis of Topology Design due to Linear Elastic Analysis	Topology Design due to Nonlinear Elastic Analysis
1	2.073×10^{-2}	2.072×10^{-2}
10	2.073	2.070
100	2.072×10^{2}	2.067×10^{2}
300	1.865×10^{3}	1.862×10^{3}
500	5.176×10^{3}	4.880×10^{3}
1000	2.064×10^{4}	2.023×10^{4}

Table 1: Compliance results.

5. Compliant Mechanisms

The formulation of the structural topology optimization problem is extended to design compliant mechanisms. In previous work, compliant mechanisms have been designed under the linear assumption.[8,9] We consider geometric and material nonlinearities.

In contrast to the structural topology optimization problem where the problem is posed independent of the structure, i.e. equations 29–32, the design of compliant mechanisms is problem dependent. Typical objectives are to meet a prescribed mechanical advantage and/or geometric advantage subject to structural integrity considerations. In addition, forces, displacements, and resources are constrained.

Nonlinear springs are introduced to represent the workpiece on which the mechanism acts. Such springs, easily accommodated in the nonlinear analysis, can model the clearance between the mechanism and the workpiece and the stiffness of the workpiece. In this way, the force on the workpiece and the output displacement of the mechanism are simultaneously controlled.

As an example, we design a mechanical gripper (refer to Figure 12). The symmetric half of the $150mm \times 100mm$ domain is discretized by 1626 4-noded quadrilateral elements. A $50mm \times 40mm$ space accepts the workpiece to be gripped. A nonlinear spring is defined to simulate a clearance of

Copyright © 1998, American Institute of Aeronautics and Astronautics, Inc.

$5mm$ between the gripper and the workpiece and the linear stiffness of $k = 15N/mm$ of the workpiece as seen in Figure 13. The material response is given by equation 6 where the Young's modulus $E = 3000N/mm^2$, the Poisson's ratio $\nu = 0.4$, and the material behavior parameter $\beta = 1$.

The objective is to synthesize the topology such that the gripper applies a $F_{out} = 15N$ gripping force or the equivalent of a $1mm$ penetration into the workpiece, i.e. $u^*_{out} = 6mm$. An input force of $F_{in} = 100N$ is applied to the gripper. An upper bound on the input displacement, $u^*_{in} = 4mm$, restricts the motion and hence the external work performed on the mechanism. A lower bound on the mass, i.e. $m^{LB} \approx 20\%$ of the original domain mass, is applied to ensure that the mechanism can support the loads. An upper bound, i.e. $m^{UB} \approx 30\%$ of the original domain mass conserves resources. The penalty parameter p is incremented in steps of 0.1 from 3.0 to 5.0 to penalize intermediate densities. The density design variables are fixed as solid material, i.e. $d_j = 1$, at the input and output ports. The design variables throughout the rest of the domain are initially equated to $d_j = 0.3$, therefore the initial design is feasible. With regard to equations 23–25,

$$\Theta_1 = (u_{out} - u^*_{out})^2 \quad (33)$$

$$\Theta_2 = u_{in} - u^*_{in} \quad (34)$$

$$\Theta_3 = m - m^{UB} \quad (35)$$

$$\Theta_4 = m^{LB} - m \quad (36)$$

$$d_j{}^{LB} = 0 \quad (37)$$

$$d_j{}^{UB} = 1 \quad (38)$$

The symmetric half of the resulting topology is depicted in its initial and deformed configurations in Figures 14 and 15. Note that we only analyze the final configuration of the mechanism. A dynamic analysis is necessary to guarantee a suitable motion between the initial and final configurations.

6. Conclusion

Topology optimization of structures and compliant mechanisms undergoing large displacements requires nonlinear analysis to accommodate geometric, and possibly material, nonlinearities. A Gaussian-weighted density measure is introduced to regularize the topology optimization problem. Topology optimization using linear elastic analyses results in load independent designs. However, designs undergoing large displacements violate the linear assumption, and it is shown that the performance of the structural design can be improved by accounting for the nonlinearities. Since the topologies due to the nonlinear elastic formulation are load dependent, multiple load cases are necessary to design the optimal topology. A method to design compliant mechanisms is also presented, and the approach is demonstrated by a mechanical gripper example.

7. Acknowledgments

The authors thank Profs. Ole Sigmund, Martin Bendsøe, and Pauli Pedersen from the Technical University of Denmark, Lyngby for their insightful contributions to the direction of this work. We are grateful for the generous financial support provided the National Science Foundation (Grant #DDM93-58132NYI) and by the Danish Research Academy. The majority of this work was completed while Mr. Bruns was enrolled in the DCAMM International Graduate Research School and Prof. Tortorelli was on sabbatical leave in the Solids Mechanics Department at the Technical University of Denmark.

References

[1] M. P. Bendsøe and C. A. M. Soares, editors. *Topology Design of Structures.* NATO ASI Series. Kluwer Academic Publishers, Boston, 1993.

[2] M. P. Bendsøe. *Optimization of Structural Topology, Shape, and Material.* Springer-Verlag, New York, 1995.

[3] E. J. Haug. *Computer-Aided Kinematics and Dynamics of Mechanical Systems, Volume I: Basic Methods.* Allyn and Bacon, Boston, 1989.

[4] A. A. Shabana. *Dynamics of Multibody Systems.* John Wiley and Sons, New York, 1989.

[5] E. J. Haug, editor. *Computer Aided Analysis and Optimization of Mechanical System Dynamics.* Springer-Verlag, New York, 1984.

[6] M. F. O. Pereira and J. A. C. Ambrósio, editors. *Computer-Aided Analysis of Rigid and Flexible Mechanical Systems.* NATO ASI Series. Kluwer Academic Publishers, Boston, 1994.

[7] A. G. Erdman, editor. *Modern Kinematics: Developments in the Last Forty Years.* John Wiley and Sons, New York, 1993.

Copyright © 1998, American Institute of Aeronautics and Astronautics, Inc.

[8] O. Sigmund. On the design of compliant mechanisms using topology optimization. *Mechanics of Structures & Machines*, 25(4):493–524, November 1997.

[9] M. I. Frecker, G. K. Ananthasuresh, S. Nishiwaki, N. Kikuchi, and S. Kota. Topological synthesis of compliant mechanisms using multicriteria optimization. *Journal of Mechanical Design, Transactions of the ASME*, 119(2):238–245, June 1997.

[10] L. L. Howell, A. Midha, and T. W. Norton. Evaluation of equivalent spring stiffness for use in a pseudo-rigid-body model of large-deflection compliant mechanisms. *Journal of Mechanical Design*, 118(1):126–131, March 1996.

[11] M. P. Bendsøe and N. Kikuchi. Generating optimal topologies in optimal design using a homogenization method. *Computational Methods in Applied Mechanics and Engineering*, 71:197–224, 1988.

[12] R. B. Haber, C. S. Jog, and M. P. Bendsøe. New approach to variable-topology shape design using a constraint on perimeter. *Structural Optimization*, 11(1–2):1–12, February 1996.

[13] J. Petersson and O. Sigmund. Slope constrained topology optimization. *International Journal for Numerical Methods in Engineering*, 41(8):1417–1434, April 1998.

[14] O. Sigmund and J. Petersson. Numerical instabilities in topology optimization: A survey on procedures dealing with checkerboards, mesh-dependencies and local minima. *To appear in Structural Optimization*, 1998.

[15] K. Svanberg. Method of moving asymptotes - a new method for structural optimization. *International Journal for Numerical Methods in Engineering*, 24(2):359–373, February 1987.

[16] P. Michaleris, D. A. Tortorelli, and C. Vidal. Tangent operators and design sensitivity formulations for transient non-linear coupled problems with applications to elastoplasticity. *International Journal for Numerical Methods in Engineering*, 37(14):2471–2499, 1994.

[17] D. E. Smith, D. A. Tortorelli, and C. L. Tucker III. Optimal design for polymer extrusion. Part I: Sensitivity analysis for nonlinear steady-state systems. *To appear in Computer Methods in Applied Mechanics and Engineering*, 1998.

Figure 6: Topology plot of the density measures, $\bar{\eta}(\mathbf{d})$. Nonlinear elastic analysis with $P = 1N$.

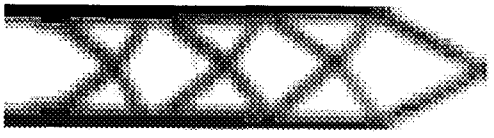

Figure 7: Topology plot of the density measures, $\bar{\eta}(\mathbf{d})$. Nonlinear elastic analysis with $P = 10N$.

Figure 8: Topology plot of the density measures, $\bar{\eta}(\mathbf{d})$. Nonlinear elastic analysis with $P = 100N$.

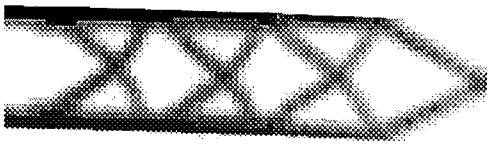

Figure 9: Topology plot of the density measures, $\bar{\eta}(\mathbf{d})$. Nonlinear elastic analysis with $P = 300N$.

Figure 10: Topology plot of the density measures, $\bar{\eta}(\mathbf{d})$. Nonlinear elastic analysis with $P = 500N$.

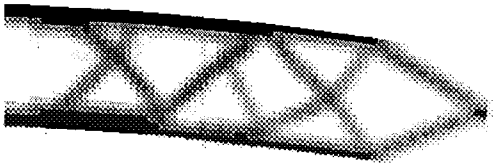

Figure 11: Topology plot of the density measures, $\bar{\eta}(\mathbf{d})$. Nonlinear elastic analysis with $P = 1000N$.

Copyright © 1998, American Institute of Aeronautics and Astronautics, Inc.

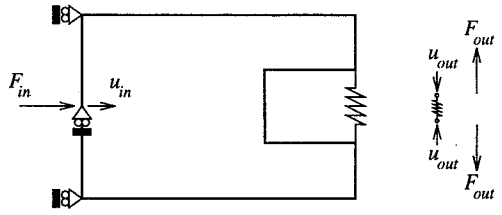

Figure 12: Mechanical gripper.

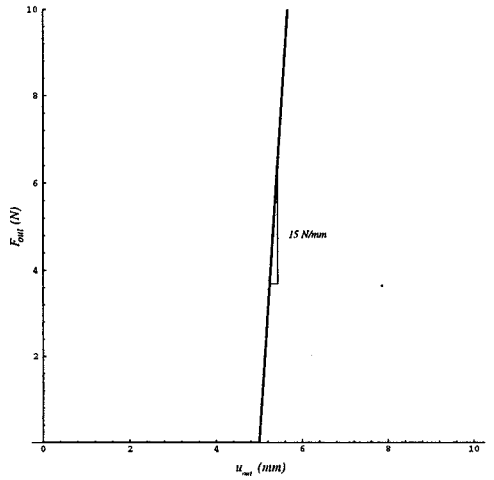

Figure 13: Nonlinear spring response.

Figure 14: Symmetric half of mechanical gripper in initial configuration. Topology plot of the density measures, $\bar{\boldsymbol{\eta}}(\mathbf{d})$.

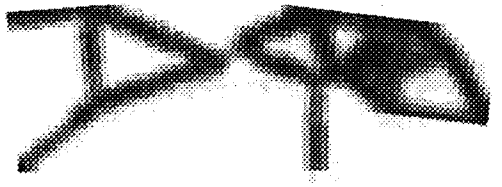

Figure 15: Symmetric half of mechanical gripper in deformed configuration. Topology plot of the density measures, $\bar{\boldsymbol{\eta}}(\mathbf{d})$.